PHYSICAL REVIEW B VOLUME 16, NUMBER 4 15 AUGUST 1977

# Chlorine chemisorption on silicon and germanium surfaces: Photoemission polarization effects with synchrotron radiation

J. E. Rowe, G. Margaritondo,* and S. B. Christman
*Bell Laboratories, Murray Hill, New Jersey 07974*
(Received 29 April 1977)

The electronic states due to saturation Cl coverage on Si(111)2 × 1, Si(111)7 × 7, Si(100)2 × 1, and Ge(111)2 × 1 surfaces have been investigated with uv photoemission techniques employing synchrotron radiation. The energy position of the Cl-induced peaks in the photoemission spectra did not provide enough information to clearly identify the chemisorption geometry for each surface. Photon polarization effects have helped to solve this problem by determining the energy position of the $p_z$-like contributions to the density of filled states. The Cl adatoms have been found to occupy covalent onefold coordinated sites on Si(111)2 × 1 and threefold ionic sites on Ge(111)2 × 1. Both the above configurations coexist on Si(111)7 × 7, while for Si(100)2 × 1 the Cl-Si bonds are still covalent, but they are probably tilted with respect to the surface normal. Constant-initial-state curves reveal three Cl-induced structures in the density of empty states above the vacuum level. None of these empty state peaks seems to be related to the $\sigma$-antibonding states of the Si-Cl covalent bond on Si(111)2 × 1 which are therefore probably located below the vacuum level.

## I. INTRODUCTION

Ultraviolet photoemission spectroscopy (UPS) is a widely employed experimental method to study chemisorption processes.[1] In most cases only a few of several possible UPS techniques have been employed for chemisorption studies. The number of available UPS techniques has been recently expanded by the use of synchrotron radiation as a continuous and polarized uv source.[2] In the present work, synchrotron-radiation photoemission spectroscopy has been successfully applied to the study of Cl-covered germanium and silicon surfaces. In particular, photon polarization effects observed in the photoemission spectra have allowed us to determine the Cl chemisorption site for several of these surfaces while neither conventional UPS techniques nor simple chemical arguments had been able to completely solve this problem. It has been found that on Si(111)2 × 1, the chlorine adatoms sit on top of the substrate atoms of the first layer in a onefold coordinated covalent site. On Ge(111)2 × 1 the adatoms go into "interstitial," threefold coordinated "ionic" positions. More complicated situations have been found for Cl-covered Si(111)7 × 7 and Si(100)2 × 1 surfaces. Both the above chemisorption geometries appear to coexist on the former, and mostly covalent Cl-Si bonds at a large angle with respect to the surface normal are established on the latter.

Recent extensive studies of hydrogen chemisorption on Si(111) surfaces[3] have demonstrated that even for a simple atom such as hydrogen the chemisorption process may be rather complicated and not easily predicted on chemical grounds. For chlorine chemisorption the situation is even more complicated; on (111) surfaces the large electronegativity difference ($\Delta\chi \approx 1.2$) between chemisorbed and substrate atoms might lead each adatom to occupy a threefold coordinated site rather than being bound to a single substrate atom as would happen to a hydrogen adatom. The theoretical calculations[4,5] give similar density-of-states spectra for the two above chemisorption geometries with an intense Cl-induced peak 5–6 eV below the top of the valence band, $E_v$. Small differences between the two geometries are predicted for the remaining spectral features, but the density of states is usually distorted in the photoemission process by factors such as matrix elements so that the determination of the chemisorption site is quite difficult on the basis of such small differences. More pronounced differences between the two geometries are predicted for the wave-function character of the spectral features. The theoretical density of filled states contributions from $p_z$-like atomic orbitals is nearly degenerate with the $p_x$, $p_y$ states for the threefold Cl chemisorption geometry, while the $p_z$ states are well separated from $p_x$, $p_y$ states at larger binding energies for the onefold geometry. Several previous examples[4,6,7] have shown that observing photon polarization effects in the photoemission spectra may be a suitable way to identify $p_z$-like contributions to the density of filled states. In order to do that one is required to separate the *true* polarization effects from spurious effects related to changes in the angular photoelectron collection geometry while changing the photon polarization.[7] In most of the present experiments we have employed an angle-integrated collection geometry, and this geometry has been kept constant while

changing the photon polarization. In some experiments, only photoelectrons emitted normal to the sample surface have been selected in order to further extend the information from angle-integrated spectra. Photon polarization-dependent energy distribution curves (EDC's) have been studied over a large range of photon energies to separate initial- and final-state effects. The density of empty states has been investigated by means of constant-initial-state (CIS) curves.[8] In this way detailed knowledge of the Cl-induced electronic structure has been achieved and these results have been explained with the current theoretical calculations[4,5] for Si(111)1 × 1 + Cl.

## II. EXPERIMENTAL PROCEDURE

The uv photoemission source employed in the present experiment was the University of Wisconsin storage ring.[9] A stainless-steel bakable vertical Seya-Namioka monochromator was used to obtain continuously tunable uv photons in the energy range $\hbar\omega = 7-65$ eV. The resulting photon beam was linearly polarized with the electric vector parallel to the horizontal plane and the polarization was greater than 98%. The beam reached the sample at an angle of incidence of 45°, and the resulting photoelectrons were collected and analyzed in energy by means of a cylindrical mirror analyzer (CMA). The CMA axis was in the plane of incidence of the photons and perpendicular to the photon beam line and therefore at 45° with respect to the sample normal.[7] The two normal modes of photon polarization have been employed. The first had the electric vector of the radiation perpendicular to the plane of incidence and therefore parallel to the sample surface, i.e., $E_z = 0$ ($s$ polarization). The second had the electric vector parallel to the plane of incidence, i.e., $E_z \neq 0$ ($p$ polarization). Switching from one polarization to the other was accomplished by rotating the sample and sample chamber around the beam line. In order to avoid changes in the photoelectron collection geometry and subsequent spurious effects due to the photoelectron angular distribution, the CMA had to be rigidly rotated with the sample. The ultrahigh vacuum of the chamber (base pressure $1 \times 10^{-10}$ Torr, working pressure $5-10 \times 10^{-10}$ Torr) was maintained while performing the rotation by a double differentially-pumped rotatable joint connecting the chamber to the beam line. The rise in pressure during the rotation was less than a factor of 3 above the working pressure.[10]

The photoelectron energy analysis was performed either in the EDC mode, keeping constant the photon energy $\hbar\omega$ and sweeping the electron energy $E$, or, in the constant-initial-state (CIS)[8] mode, sweeping both these quantities, but keeping constant their difference $\hbar\omega - E$. It is known that the EDC's are mostly related to the density of initial states[1] for $\hbar\omega \geq 20-25$ eV, while it has been demonstrated in several cases[7,8,11] that most of the CIS curve features are related to structure in the density of final states. As mentioned above, some of the EDC's and CIS curves were taken in a "normal emission" collection geometry. Photoelectrons emitted within ±5° from the normal direction to the substrate were selected in that case by means of a metal shield with a small hole in front of the CMA.

Clean reconstructed Si(111)2 × 1 and Ge(111)2 × 1 surfaces have been prepared by *in situ* cleaving under ultrahigh vacuum conditions, while Si(111)7 × 7 and Si(100)2 × 1 have been obtained by annealing to ~1250 °C and slow cooling. Saturation Cl coverages have been achieved after exposures in the range 10–200 L (1 langmuir = $10^{-6}$ Torr sec). The saturation-exposure chlorine-covered surfaces proved to be extremely stable and no surface contamination was detected by Auger electron spectroscopy after a period of more than one week at pressures less than $1 \times 10^{-9}$ Torr. The surface contamination by unwanted impurities was below $10^{-2}$ monolayers as given by Auger electron spectroscopy for all the results we present in this paper.

## III. EXPERIMENTAL RESULTS: PHOTOEMISSION SPECTRA

For all the surfaces studied, the chlorine adatoms produced a strong peak in the EDC's ~5–6 eV below $E_v$. Additional structure has been detected ~4.7 eV below $E_v$ for Ge, and 4.5–5, 2–3, and 8.9–9.5 eV below $E_v$ for Si. This similarity for all the surfaces might lead one to conclude that the Cl chemisorption process is somewhat independent of the structural properties of the substrate and of its reconstruction. As we shall see this is *not* true, and only photon polarization effects emphasize the structural differences of chemisorbed Cl on each surface. Low-energy electron diffraction data show that at this saturation stage of the chlorination process the Si(111) and Ge(111) surfaces exhibit primitive 1 × 1 patterns, while the 2 × 1 character is still present for Si(100)2 × 1.[12]

Photoelectron EDC's of several Cl-covered Si surfaces are shown in Figs. 1–5 for a number of photon energies and both polarization modes. Figures 1 and 2 show angle-integrated data for initial surfaces Si(111)2 × 1 and Si(100)2 × 1, respectively. Figure 3 includes normal-emission data as well as angle-integrated data for Si(111)7 × 7, while Figs. 4 and 5 show normal-emission data for

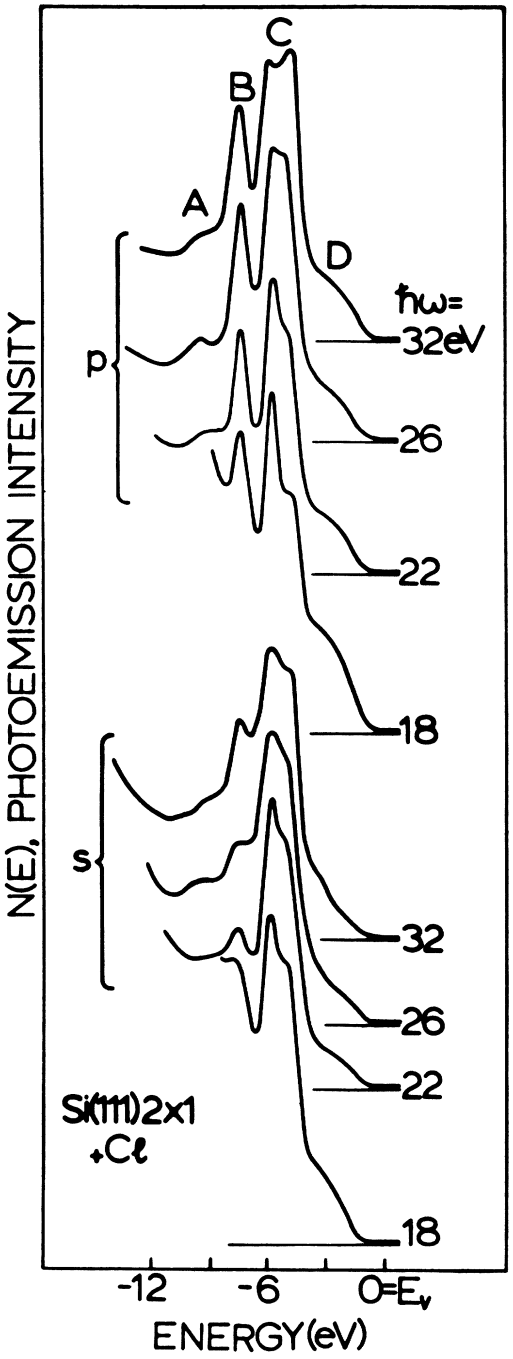


FIG. 1. Angle-integrated EDC's for the chlorine covered Si(111)2×1 surface taken for several photon energies and both $s$ and $p$ polarizations. The curves have been normalized to have the same intensity for peak C.

Si(111)2×1 and Si(100)2×1. In general, the normal-emission results show sharper features than do the corresponding angle-integrated spectra. Figure 6 shows the EDC's of Ge(111)2×1+Cl at a photon energy $\hbar\omega = 24$ eV. It is quite clear from

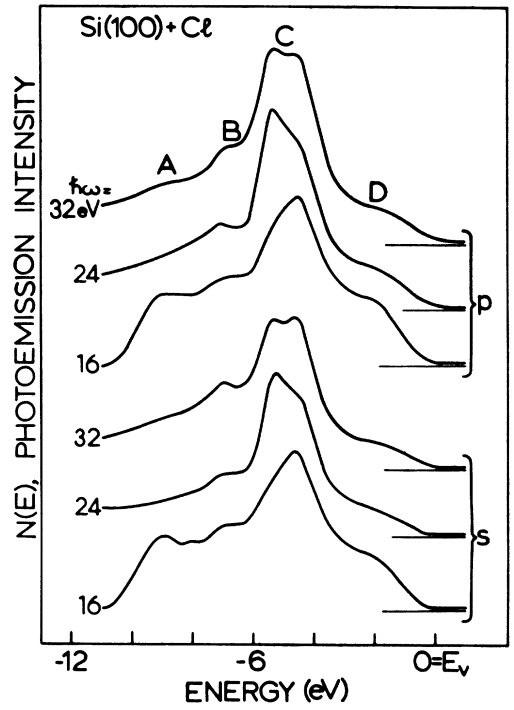


FIG. 2. Angle-integrated EDC's for chlorine covered Si(100)2×1.

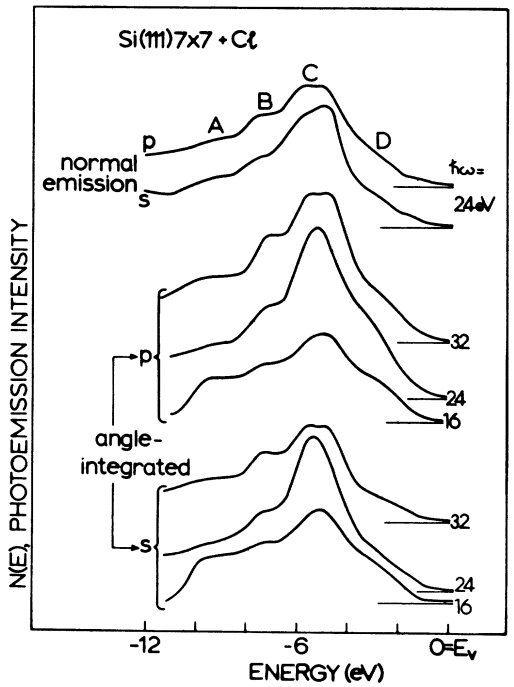


FIG. 3. Angle-integrated and normal-emission EDC's for Si(111)7×7+Cl. No normalization has been performed in this case.

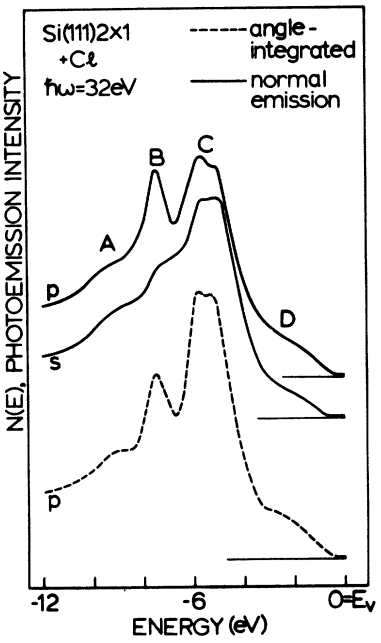


FIG. 4. Comparison between angle-integrated (dashed curve) and normal-emission (solid line) EDC's for Si(111)2×1+Cl.

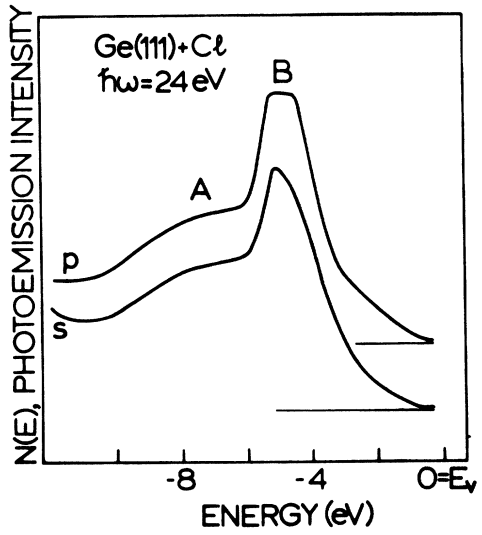


FIG. 6. Angle-integrated EDC's for Ge(111)2×1+Cl at a photon energy $\hbar\omega = 24$ eV and for $s$ and $p$ polarizations.

Figs. 1–6 that the energy position of the EDC peaks does not depend much on the photon energy. The peak positions are also approximately the same in both angle-integrated and normal-emission EDC's. Thus final-state effects only affect the relative intensity of the spectral features.

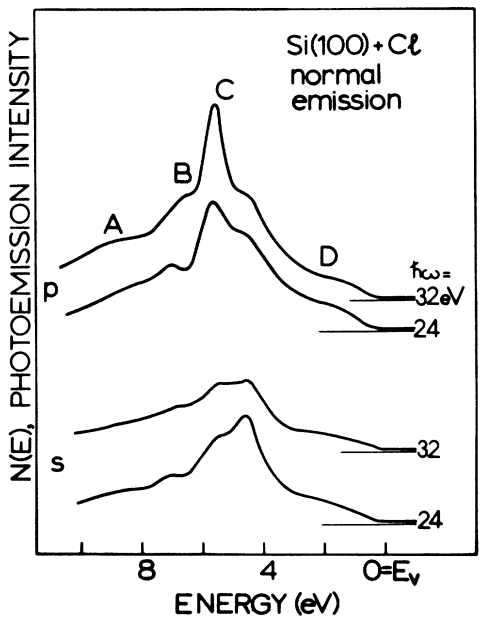


FIG. 5. Normal-emission EDC's for Si(100)2×1+Cl.

The most pronounced polarization effects occur for Si(111)2×1 and for Ge(111)2×1. Figure 1 shows that the relative intensity of peak B dramatically decreases while changing the polarization from $p$ to $s$ modes for cleaved Si(111)2×1. The same effect can be observed in Fig. 4 for the normal-emission EDC's of this surface. Figure 6 shows that the main peak of the cleaved Ge(111)2×1+Cl EDC's is asymmetrically narrowed by switching from $p$ to $s$ polarization, and its high-energy side becomes much less intense than the low-energy one. Much weaker polarization effects are observed in the angle-integrated EDC's of Si(111)7×7+Cl (Fig. 2) and Si(100)2×1+Cl (Fig. 3). Figure 2 shows that for Si(111)7×7+Cl the polarization effects are weak in the normal emission EDC's, too. Strong polarization effects are instead present in the normal-emission EDC's of Si(100)2×1+Cl, and one can see from Fig. 5 that they are quite different from those observed for Si(111)2×1+Cl.

Figures 7 and 8 show the CIS curves for chlorinated Si(111)2×1 and Si(111)7×7, Si(100)2×1 and Ge(111)2×1, respectively. For each CIS curve a different value of the initial-state energy [i.e., constant difference $(\hbar\omega - E)$] has been employed, corresponding to a different initial state of the optical transition giving rise to primary photoemission.[8] The initial-state energy has always been selected to coincide with one of the peaks in the EDC's. In this way one selects a maximum in the density of initial states, and the condition for having a peak in the CIS curves is to have a maximum in the density of final states too.[11] The CIS

peaks should then correspond to maxima in the conduction-band density-of-states modified by the Cl adatoms. The CIS curves of Fig. 7 have been taken for three different initial-state energies, the first one corresponding to peak B in the EDC's of Fig. 1, and the other two to the two lobes of peak C. All the CIS curves have been plotted as a function of the *final*-state energy. Three Cl-related structures have been revealed in this way at 6.5, 8.7, and 10.3 eV above $E_v$, peaks $\alpha$, $\beta$, and $\gamma$, respectively. These structures are clearly due to the adatoms since the conduction-band density of states for clean silicon is rather smooth and free-electron-like. Weaker structures than for the Si(111)2 $\times$ 1 CIS curves are observed in Fig. 8 for the other three chlorinated surfaces. A shoulder is still present at an energy position close to peak $\alpha$ of Fig. 7. A broad band is centered around the energy position of peak $\gamma$, and it also overlaps peak $\beta$.

The energy positions of EDC and CIS structures have been summarized in Table I for the silicon surfaces, and in Table II for germanium. We have attempted to correlate the Si(111)2 $\times$ 1 + Cl energy positions of Table I to the Cl-induced transition energies observed for this surface with elec-

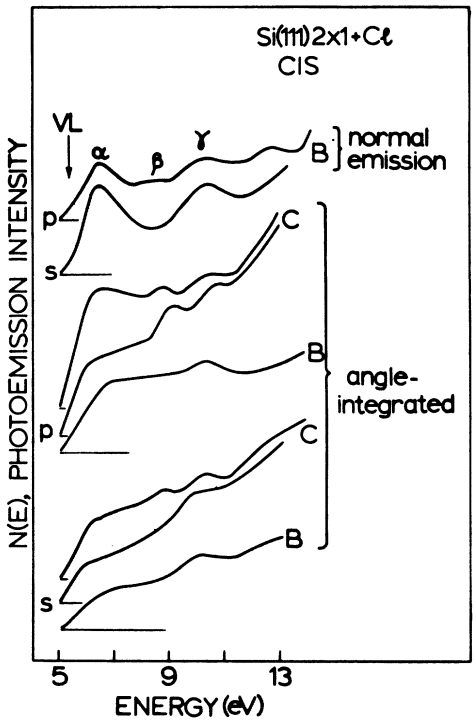


FIG. 7. CIS curves for Si(111)2 $\times$ 1 + Cl plotted as a function of the *final* state energy (VL, vacuum level). The initial state is indicated on the side of each curve. For angle-integrated CIS curves labeled as originating from peak C in EDC's the initial-state energy has been selected to correspond either to the low- or to the high-energy lobe of that peak. Both the resulting curves are shown for each polarization and the lower one corresponds to the low-energy lobe.

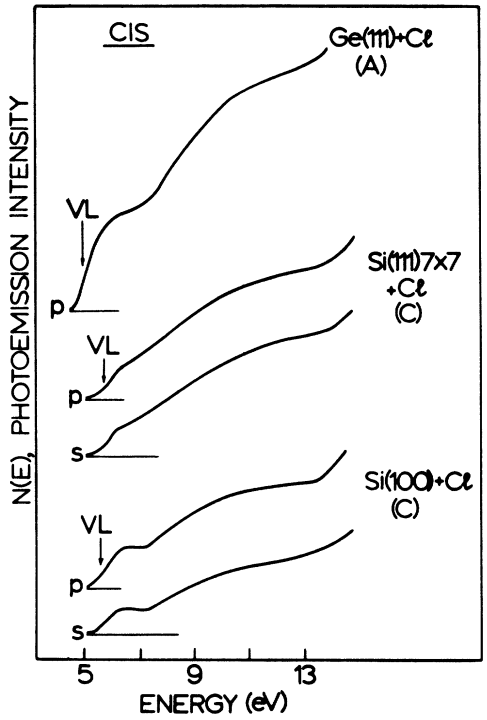


FIG. 8. CIS curves for chlorine-covered Ge(111)2 $\times$ 1, Si(111)7 $\times$ 7, and Si(100)2 $\times$ 1. The initial-state energy for the latter two has been selected to coincide with the center of gravity of peak C. We observe that the shoulder above the vacuum level VL present for all the curves has roughly the same position as peak $\alpha$ of Fig. 7. The broad band above it overlaps peak $\beta$ and peak $\gamma$ and it is centered around the position of peak $\gamma$.

TABLE I. Energy position of the EDC and CIS peaks for saturation chlorine exposure on Si surfaces.[a]

| Peak | Si(111)2 $\times$ 1 | Si(111)7 $\times$ 7 | Si(100)2 $\times$ 1 |
|---|---|---|---|
| A | 9.4 $\pm$ 0.3 | 9.4 $\pm$ 0.3 | 8.9 $\pm$ 0.4 |
| B | 7.5 $\pm$ 0.3 | 7.3 $\pm$ 0.3 | 7.0 $\pm$ 0.2 |
| C | 5.4 $\pm$ 0.4 | 5.1 $\pm$ 0.4 | 5.0 $\pm$ 0.4 |
| D | 2.7 $\pm$ 0.4 | 2.5 $\pm$ 0.4 | 2.1 $\pm$ 0.4 |
| Vacuum level | 5.5 $\pm$ 0.2 | 5.8 $\pm$ 0.2 | 5.6 $\pm$ 0.2 |
| $\alpha$ | 6.5 $\pm$ 0.4 | ~6.5 $\pm$ 0.4 | ~6.2 $\pm$ 0.4 |
| $\beta$ | 8.9 0.4 | broad band | broad band |
| $\gamma$ | 10.3 $\pm$ 0.4 | centered around 10.5 | centered around 10.3 |

[a] Positions in eV with respect to $E_v$. The experimental uncertainty is due in part to the dispersion with $\hbar\omega$ of the experimental peaks. For peak C the position here reported is the center of gravity of its two lobes.

TABLE II. Energy position of the EDC and CIS peaks for saturation chlorinate exposure on Ge(111)2×1.

| Peak | Position[a] |
|---|---|
| A | 7.5±0.6 |
| B | 4.7±0.4 |
| Vacuum level | |
| $\alpha$ | 6.5±0.4 |
| $\beta+\gamma$ | broad band centered around 10.4 |

[a] Positions in eV, with respect to $E_v$. The experimental uncertainty is due in part to the dispersion with $\hbar\omega$ of the experimental peaks. For peak C the position here reported is the center of gravity of its two lobes.

tron-energy-loss spectroscopy.[12] Among the five transition energies 3.5, 5, 9, 11.5, and 13.5 eV reported in Ref. 12 the first two are too small to have the final state above the vacuum level [5.8 eV above $E_v$ for chlorinated Si(111)2×1]. Our CIS technique cannot of course reveal density-of-state peaks in the conduction band below the vacuum level. The last three transition energies correspond within the experimental uncertainty to the energy difference between the CIS peak $\alpha$ and the EDC peaks D, C, and B, respectively.

## IV. DISCUSSION

### A. Si(111)2×1 and Si(111)7×7

The attempt to determine *a priori* the most probable chemisorption site for Cl on Si(111) on simple chemical grounds leads to inconclusive results. The similarity with hydrogen[3] suggests assuming that each Cl adatom sits on top of a silicon atom of the outermost layer and that it saturates its dangling bond, giving rise to a covalent Cl-Si bond. This, however, may be prevented by the large Si-Cl electronegativity difference which favors a more ionic configuration. Another chemisorption geometry for halogens on (111) metal surfaces[13] is the "interstitial" threefold coordinated hollow site where the adatom sits between the three substrate atoms of the second layer. In this case, a large charge transfer occurs between the adatom and the dangling bonds of the three surrounding substrate atoms of the first layer in order to approach the closed-shell noble-gas configuration of the Cl ion. Theoretical calculations for these two geometries have been carried out by Schluter, Ho, and Cohen[4] with a self-consistent pseudopotential technique. Some of their conclusions have been confirmed by tight-binding results of K. C. Pandey.[5] Figure 9 shows the theoretical density of filled states close to the top of the valence band of a monolayer chlorinated Si(111)1×1 surface obtained by Schluter *et al.*[4] for the two configurations. One can see that in both cases chlorine produces a big peak approximately 4 to 6 eV below $E_v$. The main difference between the two curves is the presence of the narrow peak B for the onefold geometry which is not present for the threefold one. The narrowness of this peak resembles that of the experimental peak B for Si(111)2×1+Cl, but this is not a strong enough argument to support the onefold geometry on this surface beyond any doubt since the theoretical energy position of peak B (~8.5 eV below $E_v$) does not quantitatively agree with the experimental one. A much stronger argument may be obtained by examining the charge-density distribution and the atomic orbital character of each density-of-states peak.[14] For both configurations, the Cl $p_x$ and $p_y$ states contribute to the main peak C. For the threefold geometry, peak C also contains Cl $p_z$-like contributions, and these states are not completely degenerate with $p_x$ and $p_y$ since their center of gravity is at somewhat *higher* energies, ~4 eV below $E_v$. For the onefold geometry, the approximate $p_z$, $p_x$-$p_y$ degeneracy is completely removed, and the Cl $p_z$ states to-

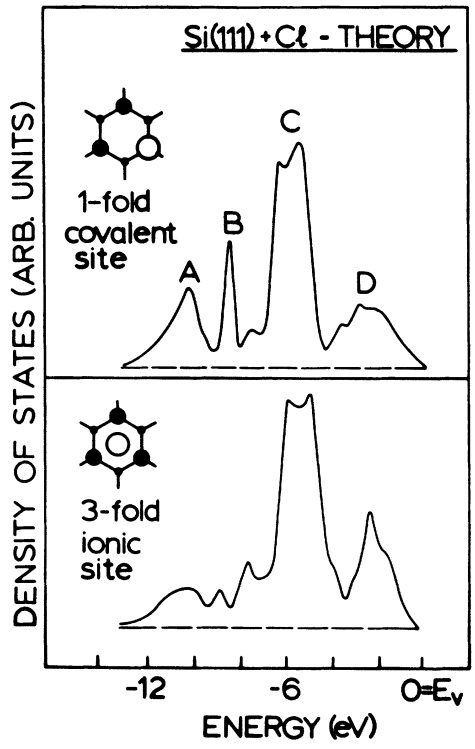


FIG. 9. Theoretical density of filled states calculated by Schluter, Ho, and Cohen (Ref. 4). The surface is a chlorine monolayer coverage of Si(111)1×1 and each of the two curves corresponds to the chemisorption site shown on the inset.

gether with Si $p_z$ states give rise to the narrow peak B. In this latter case, peak B may be regarded as a $\sigma$-like bond, and peak C as due to $\pi$-bonding states. For the onefold geometry, some $p_z$-like contribution is also expected at lower energies than peak B, and this corresponds to an enhancement of the Si $s$ states which gives rise to peak A. For both configurations peak D corresponds to Cl-perturbed $p$-like Si-Si bonds. In summary, the relative position of the Cl $p_z$-like states with respect to the $p_x$ and $p_y$ states is the main difference between the two proposed chemisorption geometries.

Previous results for III–VI layer compounds[6,7] have shown that the $p_z$-like states can be identified in angle-integrated photoemission spectroscopy on the basis of their polarization dependence. In our case, a $p_z$-like character for peak B of Si(111)2×1+Cl can be deduced from its much weaker intensity for $s$ than for $p$ polarization. This can be easily understood if one makes the simple assumption of plane-wave final states, which in this case is supported by the nearly-free-electron-like behavior of the CIS curves at these energies. A more detailed analysis[7] shows that the polarization dependence of peak B in Fig. 1 may be explained either by a marked $p_x$, $p_y$ character corresponding to $d_{z^2}$-like final states or by a marked $p_z$-like character corresponding to any combination of $s$, $d_{xz}$, and $d_{yz}$ final states.[15] One cannot exclude a $d_{z^2}$-like character to prevail over a *small* energy range in the final states. This implies that one has to be extremely careful while interpreting polarization effects that only occur for a small photon energy range. Therefore we have limited our analysis to polarization effects that occur over a *large* photon energy range. Such is the case of peak B in Fig. 1, and we conclude that only a $p_z$-like character can explain its polarization dependence. This conclusion agrees with the above theories[4] since none of them predicts a Cl $p_x$, $p_y$ contribution at energies below the main peak C. The onefold geometry results do predict a $p_z$-like character for peak B and we conclude that this geometry prevails for Si(111)2×1+Cl. More arguments in favor of this conclusion are obtained from the normal-emission spectra of Fig. 4. There we see that the $p$-polarization peak B is enhanced while one changes the collection geometry from angle-integrated to normal emission. Again, assuming plane-wave final states, the angular dependence of $p_z$-like contributions to the EDC's has a maximum for normal emission.[16]

The above conclusions for Si(111)2×1+Cl cannot be extended to Si(111)7×7+Cl since much weaker polarization effects are observed in Fig. 2 than in Figs. 1 and 4. A pure threefold geometry can also be excluded for this surface since it would correspond to strong polarization effects for the high-energy side of peak C where the $p_z$-like contributions are predicted to be in this case. We observe that the energy positions of the Si(111)7×7+Cl EDC peaks are not too dissimilar from those of Si(111)2×1+Cl nor from those generally predicted by the above theoretical calculations for the two proposed chemisorption geometries. Therefore a third chemisorption geometry completely different from the two previously proposed does not seem likely. We rather believe that *both* the onefold and the threefold configurations are present at the same time on Si(111)7×7+Cl. This is supported by several arguments. Some weak polarization effect is still present in the normal-emission EDC's of Fig. 2 for peak B and this peak is again enhanced by the normal-emission geometry. Angle-of-incidence effects for peak B have been observed by Sakurai *et al.*[12] on annealed Si(111)7×7+Cl which indicate that peak B is still polarization dependent to some extent. Thus, Cl adatoms in onefold sites are present on Si(111)7×7. However, there may exist more than one ordered phase for saturation Cl-covered Si(111)7×7. Low-energy electron diffraction results in progress indicate the possibility of at least three separate phases of chemisorbed Cl on this surface. Thus it is quite likely that Sakurai *et al.* selectively obtained the phase with a high percentage of onefold Cl sites. Our present results for annealed Si(111)7×7+Cl show that peak C is broader and peak D larger than for cleaved Si(111)2×1+Cl. Figure 9 shows that this broadening is peculiar to the threefold geometry. Thus Cl adatoms on threefold sites are also present on the annealed Si(111)7×7 surfaces we obtained in the present experiments.

A qualitative model for the coexistence of both chemisorption geometries on Si(111)7×7 can be based on the well-known vacancy model for the 7×7 reconstruction.[17] Chlorine adatoms absorbed at surface vacancies are in a geometry similar to that of chemisorbed adatoms on a threefold site of the perfect surface. At the same time the onefold site prevails on the remainder of the surface as it does on Si(111)2×1.

The CIS results of Figs. 7 and 8 for chlorinated Si(111) surfaces cannot be fully explained at this time since no theoretical results are currently available for the density of empty states above the vacuum level. Simple chemical reasoning suggests that on Si(111)2×1+Cl an important contribution to the density of empty states must be coming from the antibonding partner of the $\sigma$-bonding states (peak B). None of the three CIS structures $\alpha$, $\beta$, and $\gamma$ of Fig. 7 seems to correspond to these states which are theoretically predicted at lower ener-

gies below the vacuum level.[5] Evidence for a peak in the density-of-states structures below the vacuum level on Si(111)7×7+Cl is provided by electron-energy-loss data.[12] Indeed the Cl-induced transition observed for Si(111)7×7 at ~5 eV must have the Cl-enhanced peak D as an initial state, and the final state 2.3 eV above $E_v$. This is in reasonable agreement with the theoretically predicted energy position of the σ-antibonding Si-Cl states. Therefore we conclude that the energy-loss transition at ~5 eV involves the antibonding σ states of the fraction of Cl adatoms that occupy onefold sites on Si(111)7×7. Similar unoccupied states are likely to be present for Si(111)2×1+Cl where the covalent onefold geometry prevails. The last energy-loss peak observed for Si(111)7×7+Cl may also have peak D for an initial state, with the final state at 0.8±0.5 eV above $E_v$, i.e., it coincides with the conduction-band edge within the experimental uncertainty. The origin of the CIS peaks α, β, and γ which are clearly observed only for Si(111)2×1+Cl and only weakly visible for the other surfaces is not yet clear and its understanding will require a more complete theoretical treatment. Recent results for[7] GaSe and[11] $SnS_2$ show that these calculations are not beyond the present capabilities of pseudopotential techniques.

### B. Ge(111)2×1 with chlorine

Interpreting the results for cleaved Ge(111)2×1+Cl is as straightforward as for cleaved Si(111)2×1+Cl. Figure 6 clearly shows that for *s* polarization the high-energy side of the main Cl-induced EDC peak almost disappears. The same effect has been observed over a large range of photon energies $\hbar\omega = 16$–$36$ eV. Therefore, the high-energy side of the main Cl-induced EDC peak is where the $p_z$-like Cl orbital contributions are concentrated. This is exactly what Schluter *et al.*[4] predict in the case of Si(111)1×1+Cl for the threefold chemisorption geometry. Due to the similarity between the silicon and germanium electronic structure of clean surfaces and the bulk, the same theory may be extended to both Ge and Si. The ionic threefold geometry occurs on the chlorinated Ge(111)2×1 surfaces. The difference we find between Cl-covered Si(111)2×1 and Ge(111)2×1 is quite unexpected because of the similarity between the two materials. A qualitative explanation can be obtained from examinations of the theoretical dangling-bond charge distributions for the clean Si(111) and Ge(111) surfaces.[14] On Si(111), each dangling-bond orbital is quite confined to the space region *above* the corresponding surface atom. On Ge(111), the dangling-bond charge distribution significantly spreads into the region where adatoms in threefold ionic sites would be. Therefore Ge more than Si may be expected to transfer its dangling-bond charge to an interstitial Cl adatom and help form the more ionic bonds of the threefold coordinated adsorption site.

The CIS spectra for Ge(111)2×1+Cl are similar to those of Si(111)7×7+Cl and essentially consist of a broadened version of the Si(111)2×1+Cl data. This confirms that the CIS structure cannot be associated with σ-antibonding states of the covalent adatom substrate atom bond since there is no evidence for the formation of these bonds on Ge(111).

### C. Si(100)2×1 with chlorine

The experimental results for chlorine-covered Si(100) exhibit the following remarkable differences with respect to either Si(111) or Ge(111). Table I shows that the energy positions of the EDC and CIS structures are systematically closer to $E_v$ for Si(100) than for Si(111). No strong polarization effects are found for the angle-integrated EDC's or CIS curves, while the normal-emission EDC's of Fig. 5 do exhibit an enhancement of *both* peaks B and C for *p* polarization. Moreover the 2×1 reconstruction for Si(100) is still present after chlorine saturation exposures, while the 7×7 and 2×1 reconstruction on Si(111) is eliminated. The Cl-induced work-function changes are small for Si(100)2×1, but larger than one electron-volt on Si(111).[12] Sakurai *et al.*[12] have proposed that the structural Si-Si pairing characteristics of the reconstructed Si(100)2×1 surface are responsible for the pecularities of the chlorine adsorption process of the (100) surface with respect to Si(111) or Si(110), and the present results seem consistent with their hypothesis. There are two dangling bonds per Si(100) surface atom, and they are at an angle of ~54° with respect to the surface. The Cl adatoms are not likely to sit on top of the first-layer Si atoms, but between them, and the Si-Cl bonds are not perpendicular to the surface, resulting in weaker polarization effects. The $p_x$, $p_y$ Cl orbitals are now expected to have more bonding character than for Si(111)2×1+Cl and to be mixed to the $p_z$-like orbitals at energies lower than peak C. The occurrence of this mixing is supported by the normal-emission polarization effects of Fig. 5 which reveal a similar character for both peak B and the low-energy lobe of peak C, and Cl $p_z$-like orbitals now contribute to both these peaks. The $p_z$-like contributions are of course enhanced by the normal-emission geometry, while in angle-integrated geometry, the mixing of $p_z$ and $p_x$, $p_y$ orbitals result in a weakening of all the polarization effects.

The CIS results for the Si(100) surface are again

similar to results for Si(111)7×7+Cl and Ge(111)2×1+Cl. In summary, the observed CIS peaks do not depend on the substrate nature, orientation, and reconstruction, and this is a further proof that they cannot be associated with specific geometric details of Cl-$X$ bonds present on Si and Ge surfaces.

## V. CONCLUSIONS

It has been shown that photon polarization effects studied over a large range of photon energies help to identify chemisorption geometries in cases when the EDC-structure energy positions do not give conclusive information alone. Contributions to the EDC's from $p_z$-like Cl orbitals have been detected at lower energies than the $p_x$, $p_y$ orbitals for Si(111)2×1+Cl, and at slightly larger energies than $p_x$,$p_y$ for Ge(111)2×1+Cl. This shows that in spite of the similarity between these two surfaces, Cl is chemisorbed in a onefold covalent site on cleaved Si(111)2×1 and in a threefold ionic site on cleaved Ge(111)2×1. The coexistence of both chemisorption sites is suggested for Si(111)7×7+Cl. For Si(100)2×1+Cl, the Cl $p_z$-like orbitals are mixed with the $p_x$, $p_y$ orbitals to some extent, and the Cl-Si bonds should appear to be covalent in character, but are tilted with respect to the sample normal. The EDC peaks for the chlorine-covered (111) surfaces have been explained on the basis of the current theoretical models for the above two chemisorption geometries. Three empty density-of-states peaks have been found above the vacuum level in the CIS curves for all surface orientations studied, and they do not seem related to any particular chemisorption geometry nor to the substrate structure. Explaining the origin of these unoccupied states requires a detailed theory of the conduction bands after chlorine adsorption.

The present experiments emphasize that UPS may be an extremely versatile technique to study chemisorption processes if one fully exploits the potential applications of synchrotron radiation. Methods similar to the one employed in the present work can be easily and usefully extended to any chemisorbed species on metal and semiconductor surfaces with a strong directional character. Among the many possible candidates a few examples are hydrogen,[3] CO (Ref. 18), and several hydrocarbon molecules which are thought to form strong chemisorption bonds with a significant $p_z$-symmetry component.[19]

---

*Postdoctoral Research Fellowship. On leave from Gruppo Nazionale de Struttura della Materia/Consiglio Nazionale delle Ricerche, Rome, Italy.

[1]See, for instance, H. D. Hagstrum, J. E. Rowe, and J. C. Tracy, in *Experimental Methods in Catalytic Research*, Vol. 3, edited by R. B. Anderson and P. T. Dawson (Academic, New York, 1976), pp. 42–120.

[2]D. E. Eastman, in *Vacuum Ultraviolet Radiation Physics*, edited by E. E. Koch (Pergamon-Vieweg, Braunschweig 1974), p. 417.

[3]K. C. Pandey, T. Sakurai, and H. D. Hagstrum, Phys. Rev. Lett. 35, 1728 (1975); H. Ibach and J. E. Rowe, Surf. Sci. 43, 481 (1974); T. Sakurai and H. D. Hagstrum, Phys. Rev. B 12, 5349 (1975).

[4]M. Schluter, J. E. Rowe, G. Margaritondo, T. M. Ho, and M. L. Cohen, Phys. Rev. Lett. 37, 1632 (1976).

[5]K. C. Pandey (private communication).

[6]J. E. Rowe, G. Margaritondo, H. Kasper, and A. Baldereschi, Solid State Commun. 20, 921 (1976).

[7]G. Margaritondo, J. E. Rowe, and S. B. Christman, Phys. Rev. B 15 (1977).

[8]G. J. Lapeyre, A. D. Baer, J. Hermanson, J. Anderson, J. A. Knapp, and P. L. Gobby, Solid State Commun. 15, 1601 (1974); G. J. Lapeyre, J. Anderson, P. L. Gobby, and J. A. Knapp, Phys. Rev. Lett. 33, 1290 (1974).

[9]The Synchrotron Radiation Center was supported by the NSF under Grant No. DMR-74-15089.

[10]A more detailed description of the experimental apparatus is reported in Ref. 7.

[11]G. Margaritondo, J. E. Rowe, M. Schluter, and A. Kasper (unpublished).

[12]T. Sakurai, J. E. Rowe, and H. D. Hagstrum (unpublished).

[13]F. Forstmann, W. Berndt, and P. Buttnes, Phys. Rev. Lett. 30, 17 (1973); G. Rovida, F. Pratesi, M. Maglietta, and E. Feroni, Jpn. J. Appl. Phys. Suppl. 2, 117 (1974).

[14]M. Schluter (private communication).

[15]As it has been discussed in Ref. 7 the dipole selection rules may not be completely valid due to the rapid space variation of the local electric field close to the surface. This explains for example why peak B of Fig. 1 is only weakened and not completely removed from $s$ polarization.

[16]R. H. Williams, P. C. Kemeny, and L. Ley, Solid State Commun. 19, 495 (1976).

[17]J. J. Lander, in *Progress in Solid Chemistry*, Vol. 2, edited by H. Reiss (Pergamon, Oxford 1965), p. 26.

[18]T. Gustafsson, E. W. Plummer, D. E. Eastman, and J. L. Freeouf, Solid State Commun. 17, 391 (1975); T. Sakurai, H. D. Hagstrum, J. E. Rowe, and G. Margaritondo (unpublished).

[19]J. E. Demuth and D. E. Eastman, Phys. Rev. B 13, 1523 (1976).